PHYSICAL REVIEW D **79,** 115013 (2009)

Leptonic radiative decay in supersymmetry without *R* parity

Chien-Yi Chen*

Department of Physics, Carnegie Mellon University, Pittsburgh, Pennsylvania 15213, USA
and Department of Physics, National Central University, Chung-Li, Taiwan 32054

Otto C. W. Kong†

Department of Physics and Center for Mathematics and Theoretical Physics, National Central University, Chung-Li, Taiwan 32054

(Received 22 January 2009; published 19 June 2009)

We present a detailed analysis together with exact numerical calculations on one-loop contributions to the branching ratio of the radiative decay of μ and τ, namely $\mu \to e\gamma$, $\tau \to e\gamma$, and $\tau \to \mu\gamma$ from supersymmetry without R parity, focusing on contributions involving bilinear couplings. A numerical study is performed to obtain explicit bounds on the parameters under the present experimental limit. We present, and use in the calculation, formulas for exact mass eigenstate effective couplings. In this sense, we present an exact analysis free from approximation for the first time. After comparing our results against the closest early analysis, we discovered a major difference in resulted constraints on some $\mu_i^* B_j$ combinations. Constraints from neutrino masses on the parameters were considered. Our result indicates that the branching ratio measurement on $\mu \to e\gamma$ down to 10^{-13}–10^{-14} and beyond, as targeted by the MEG experiment, has a chance of observing decay from the R-parity violating scenario.

DOI: 10.1103/PhysRevD.79.115013 PACS numbers: 12.60.Jv

I. INTRODUCTION

Recent neutrino experiments have demonstrated that neutrinos change flavor as they travel from source to detector, a phenomenon consistent with the hypothesis of neutrino oscillation. All that contributes evidence for neutrino masses and lepton-flavor violation (LFV) and provides the first definite experimental clue for physics beyond the standard model (SM). Many extensions of the SM predict a certain amount of LFV in relation to neutrino mass generation or otherwise. Important criterion for a viable model is giving acceptable neutrino mass spectrum while staying within experimental limits of LFV. Apart from the soft terms within the minimal supersymmetric standard model (MSSM), both LFV and neutrino masses are indeed forbidden by *ad hoc* discrete symmetry—the R parity. Note that soft terms by themselves still conserve total lepton number, and hence do not generate neutrino masses. In the supersymmetric standard model without R parity imposed, there is however an important source of LFV and neutrino masses. A major part of this comes simply from the R-parity violating (RPV) terms in the superpotential, though RPV soft (supersymmetry breaking) terms are also of interest. The latter too often escapes notice.

The best evidence of supersymmetry (SUSY) would obviously be the discovery of SUSY particles in the collider machines. However, processes such as the leptonic radiative decays can serve as alternative ways to test SUSY, complementary to the direct SUSY particle searches. Although these processes have not yet been seen so far in present experiments, there are very stringent upper bounds on their possible rates implying important constraints on the new physics contributions. The present experimental upper bounds of branching ratio for $\tau \to \mu\gamma$ [1], $\tau \to e\gamma$ [2], and $\mu \to e\gamma$ [3] are

$$\begin{aligned} \mathrm{Br}(\tau \to \mu\gamma) &< 6.8 \times 10^{-8}, \\ \mathrm{Br}(\tau \to e\gamma) &< 1.1 \times 10^{-7}, \\ \mathrm{Br}(\mu \to e\gamma) &< 1.2 \times 10^{-11}. \end{aligned}$$

The muon radiative decay reaction $\mu \to e\gamma$ has been the focus of most attention due to the experimental bound being much stronger. This bound will probably be improved in the future. The MEG experiment, Ref. [4], which searches for $\mu \to e\gamma$ decays down to 10^{-13}–10^{-14} branching ratio is now in its final stage of preparation. The τ decays may also be better probed in future facilities.

The recent studies on radiative decays from other models such as little Higgs with T parity [5,6] and the SUSY grand unified theories (GUT) [7,8] also give some interesting results on the lepton-flavor violation processes. For example, in the little Higgs models with T parity, the presence of new flavor violating interactions and mirror leptons containing masses of order 1 TeV can enhance these processes to the level of the present experimental limit. In the SUSY GUT model, Ref. [7] discusses the complementarity between lepton-flavor violation and Large Hadron Collider (LHC) experiments in probing the SUSY GUT. They found that the LFV experiments have strong capabilities to detect SUSY induced LFV, in some cases even outreaching the LHC. In Ref. [8], the authors study the correlation between U_{e3} and the $\mathrm{Br}(\mu \to e\gamma)$ in

*chienyic@andrew.cmu.edu
†otto@phy.ncu.edu.tw

the context of a SUSY SO(10) framework. They find that taking running effects into account leads to a constant enhancement of the value of U_{e3} at the high scale, bringing $\mu \to e\gamma$ into the realm of MEG for SUSY parameter space regions which were previously excluded without inclusion of such running.

The study we present in this paper analyzes branching ratios that can be generated for all processes in the context of the generic supersymmetric standard model (GSSM), i.e. SUSY without R parity [9]. If one simply takes the minimal supersymmetric field spectrum of the SM and imposes nothing more than gauge symmetries while admitting soft SUSY breaking, the generic supersymmetric standard model would be obtained. Thus, the GSSM is the complete theory of SUSY without R parity, where all kinds of RPV terms are admitted without bias. Assuming SUSY, it is at least conceptually, the simplest model to accommodate neutrino mixing and oscillations. We work within the framework of single-VEV parametrization (SVP) [9–11], which is an optimal choice of flavor basis that helps guarantee a consistent and unambiguous treatment of all kinds of admissible RPV couplings and to maintain a simple structure for RPV effects on tree-level mass matrices for all states including scalars and fermions.

The experimental bound on the branching ratio of these leptonic radiative decays is used to constrain the model parameter space, particularly the RPV part. Under constraints by the present experimental upper bound of branching ratios for $\mu \to e\gamma$, $\tau \to e\gamma$, and $\tau \to \mu\gamma$, we obtain the allowed region of the RPV parameter spaces. We give complete one-loop formulas for the type of contributions to the branching ratio of three leptonic radiative decays. We present numerical analysis of these contributions from all possible combinations of RPV parameters. Besides the more familiar $\mu_k^* \lambda_{kij}$,[1] there are a list of combinations of type $B_k^* \lambda_{kij}$, $\mu_i^* \mu_j$, and $B_i^* \mu_j$. A similar analysis on the $\mu \to e\gamma$ process has been reported in Ref. [13] in 2001.[2] The present work differs from Ref. [13] in a few important ways. The present work is based on using new formulas of exact mass eigenstate couplings to calculate the one-loop diagrams, while in Ref. [13] the authors only used electroweak states ($l_i^{\mp}$'s) as an approximation for physical particles of external legs to the loop (the charge leptons). The latter amounts to neglecting the Higgsino and wino components of the decaying and product charged leptons. Therefore, the current analysis is an improvement or completion of the work reported in Ref. [13]. In particular, we find that the constraints one can obtain on some of the $\mu_i^* B_j$ type parameter combinations have very substantial improvement. This is indeed the first exact calculation of processes within the model at the one-loop level presented, free from any approximation of the type. In addition, our results on the other two, τ decays, processes have not been available in previous literature. We also increase the value of the μ_0 parameter (corresponding to the MSSM μ parameter) used from 100 to 135 GeV to accommodate the updated lightest chargino ($\tilde{\chi}_1^{\pm}$) lower mass limit of approximately 104 GeV [19]. In the sense explained above, the paper is somewhat of a sequel to Ref. [13], where we draw comparison when relevant. However, it can also be read just on its own. Readers who want to do so may simply neglect statements matching analysis and results here with that of the latter. One catch though is that we focus our discussion and result presentations on interesting results we get beyond that of Ref. [13], only briefly summarizing features and results that are essentially well explored in the latter reference.

As experimental evidence for neutrino masses has become quite well established, we also include in our analysis a brief comparison of results from radiative decays with neutrino mass bounds. Recombinations of RPV couplings typically contribute both to the decays and neutrino masses, but with different dependence on the other model parameter. Some RPV parameters, like the bilinear ones, can give rise to a neutrino mass term alone. However, we do not have solid evidence on the scale of the neutrino masses, only Δm^2. And there are so many relevant RPV combinations for both neutrino masses and radiative decay processes that it makes a comprehensive and systematic analysis unrealistic unless further assumptions are taken on the model structure. Some parameter combinations may have a more important role to play in a certain process while others may give dominant contributions to neutrino masses. We are interested in investigating and presenting generic results on model parameters. Hence, we adopt a naive strategy on the interpretation of neutrino mass bounds as naive upper bounds on the involved parameter (s) in order not to give a neutrino mass term contribution beyond the sub-eV scale. This may be a bit on the conservative side but is considered a reasonable strategy to be adopted. Note that this rough neutrino mass scale is not expected to be pushed down, since the scale of Δm^2 is known from the oscillation experiments. On the other hand, we have only upper bounds for the radiative decays which may be, and we believe should be, probed with a lot better precision in the future. Our radiative decay results will hence be useful references for the future, even if they are no better than the naive neutrino mass bounds. In the

[1]The interesting kind of combination of bilinear and trilinear RPV parameters contributing to flavor violations through scalar mass mixings [12] or a one-loop diagram [13,14], and analogous one-loop dipole moment [15] were published a few years ago. More recently, similar contributions to radiative B decays were also published [16].

[2]There have been numerous studies on similar processes from various versions or limited models of R-parity violation in the literature. Most of the model assumptions look *ad hoc*. We have no intention of reviewing all of that here. However, an early study on $\mu \to e\gamma$ from softly broken R parity [17] should particularly be mentioned. Another particularly noteworthy paper on the topic is given by Ref. [18].

case of $\mu \to e\gamma$, for example, if the MEG experiment pushes the bound on the branching ratio down to 10^{-13}–10^{-14}, our numerical results show that it can give a stronger constraint on the $\mu_1^* B_2$ parameter combination. To put it more interestingly, the neutrino mass bounds do not rule out the possibility of seeing a $\mu \to e\gamma$ at MEG coming from $\mu_1^* B_2$ of the RPV supersymmetric model. In the case of $\mu_2^* \lambda_{212}$, the current bound is actually already competitive.

This paper is organized as follows. In the next section, we briefly summarize the main features of GSSM and also set our notation. In Sec. III, we give the general exact formulas in the basis of mass eigenstates without any approximation. The focus is on the $\ell_j^- \to \ell_i^- \gamma$ amplitude from one-loop diagrams without colored intermediate states. The two sections are included here to make the paper self-contained, and set the notation to be used for the discussions that follow. Note that Sec. III does include important results, expressions for effective coupling among mass eigenstates involved, that have not been published before. Our numerical results will be presented in Sec. IV. We also compare the results obtained by using the exact mass eigenstate couplings versus the previous calculations and discuss the sources of the difference between them. In addition, we illustrate the effects of varying the input parameters on the bounds. Finally, Sec. V will be devoted to the conclusions.

II. THE GENERIC SUPERSYMMETRIC STANDARD MODEL

We briefly describe the model here. Details of the formulation adopted are elaborated on in Ref. [9]. The most general renormalizable superpotential with the spectrum of minimal superfields can be written as

$$W = \varepsilon_{ab}[\mu_\alpha \hat{H}_u^a \hat{L}_\alpha^b + h_{ik}^u \hat{Q}_i^a \hat{H}_u^b \hat{U}_k^C + \lambda'_{\alpha jk} \hat{L}_\alpha^a \hat{Q}_j^b \hat{D}_k^C + \tfrac{1}{2}\lambda_{\alpha\beta k} \hat{L}_\alpha^a \hat{L}_\beta^b \hat{E}_k^C] + \tfrac{1}{2}\lambda''_{ijk} \hat{U}_i^C \hat{D}_j^C \hat{D}_k^C, \quad (1)$$

where (a, b) are $SU(2)$ indices, and (i, j, k) are the usual family (flavor) indices (going from 1 to 3). The (α, β) indices are extended flavor indices going from 0 to 3. Note that λ is antisymmetric in the first two indices, as required by the $SU(2)$ product rules, shown explicitly here with $\varepsilon_{12} = -\varepsilon_{21} = 1$. Similarly, λ'' is antisymmetric in the last two indices from $SU(3)_C$, though color contents are not shown here. Besides the superpotential, the Lagrangian contains the gauge interaction part, including kinetic terms of the matter superfields and a soft SUSY breaking part.

We take a definite flavor basis to write the model Lagrangian. Such choice of parametrization is not unique. In the current case of the GSSM, the scalar parts of the colorless electroweak doublet superfields could bear vacuum expectation values (VEVs). We use a parametrization called the SVP advocated by our group since Ref. [10]. A flavor basis with only one among the $\hat{L}_\alpha$'s, designated as $\hat{L}_0$, bearing a nonzero VEV is adopted. That is to say, the direction of the VEV, or the Higgs field H_d, is singled out in the four-dimensional vector space spanned by the $\hat{L}_\alpha$'s. Explicitly, under the SVP, flavor bases are chosen such that (1) $\langle \hat{L}_i \rangle \equiv 0$, which implies $\hat{L}_0 \equiv \hat{H}_d$; (2) $y^e_{jk} (\equiv \lambda_{0jk} = -\lambda_{j0k}) = \frac{\sqrt{2}}{v_0}\mathrm{diag}\{m_1, m_2, m_3\}$; (3) $y^d_{jk} (\equiv \lambda'_{0jk}) = \frac{\sqrt{2}}{v_0}\mathrm{diag}\{m_d, m_s, m_b\}$; and (4) $y^u_{ik} = \frac{\sqrt{2}}{v_u} V_{\mathrm{CKM}}^T \mathrm{diag}\{m_u, m_c, m_t\}$, where $v_0 \equiv \sqrt{2}\langle \hat{L}_0 \rangle$ and $v_u \equiv \sqrt{2}\langle \hat{H}_u \rangle$.

The soft SUSY breaking part of the Lagrangian can be written as follows [9,12]:

$$V_{\mathrm{soft}} = \epsilon_{ab} B_\alpha H_u^a \tilde{L}_\alpha^b + \epsilon_{ab}[A_{ij}^U \tilde{Q}_i^a H_u^b \tilde{U}_j^C + A_{ij}^D H_d^a \tilde{Q}_i^b \tilde{D}_j^C + A_{ij}^E H_d^a \tilde{L}_i^b \tilde{E}_j^C] + \mathrm{H.c.} + \epsilon_{ab}\left[A_{ijk}^{\lambda'} \tilde{L}_i^a \tilde{Q}_j^b \tilde{D}_k^C + \frac{1}{2} A_{ijk}^{\lambda} \tilde{L}_i^a \tilde{L}_j^b \tilde{E}_k^C\right]$$
$$+ \frac{1}{2} A_{ijk}^{\lambda''} \tilde{U}_i^C \tilde{D}_j^C \tilde{D}_k^C + \mathrm{H.c.} + \tilde{Q}^\dagger \tilde{m}_Q^2 \tilde{Q} + \tilde{U}^\dagger \tilde{m}_U^2 \tilde{U} + \tilde{D}^\dagger \tilde{m}_D^2 \tilde{D} + \tilde{L}^\dagger \tilde{m}_L^2 \tilde{L} + \tilde{E}^\dagger \tilde{m}_E^2 \tilde{E} + \tilde{m}_{H_u}^2 |H_u|^2 + \frac{M_1}{2} \tilde{B}\,\tilde{B}$$
$$+ \frac{M_2}{2} \tilde{W}\,\tilde{W} + \frac{M_3}{2} \tilde{g}\,\tilde{g} + \mathrm{H.c.}, \quad (2)$$

where we have used H_d in the place of the equivalent $\tilde{L}_0$ among the trilinear A terms. Note that $\tilde{L}^\dagger \tilde{m}_{\tilde{L}}^2 \tilde{L}$, unlike the other soft mass terms, is given by a 4×4 matrix. Compared to the MSSM case, $\tilde{m}_{L_{00}}^2$ corresponds to $\tilde{m}_{H_d}^2$, while $\tilde{m}_{L_{0k}}^2$'s give new mass mixings.

III. LEPTONIC RADIATIVE DECAYS

Within the GSSM, the three SM charged leptons are the light mass eigenstates out of a 5×5 charged fermions mass matrix, which also includes the charginos. We use the common notation $\chi_n^\pm$, $n = 1$ to 5, with the former states given by $\ell_i^\pm \equiv \chi_{i+2}^\pm$, $i = 1$ to 3. The states have characters different from the fermionic components l_i^-'s and l_i^+'s of the $\hat{L}_i$ and $\hat{E}_i^C$ superfields, respectively, as a result of the generally nonzero μ_i RPV mixings between the charged leptons and charginos of the R-parity conserving (MSSM) limit. The smallness of the μ_i values as indicated by the resulted neutrino mass value [10,20] was the basis for most of the approximations on related subject matters in the literature, essentially neglecting the difference between ℓ_i's and l_i's. Reference [13] is not totally free from the kind of approximation, though it focuses on the

$\mu_i^* \lambda_{ijk}$ RPV contributions to $\mu \to e\gamma$. We will see that in this kind of parameter combination the approximation in Ref. [13], which neglects Higgsino and wino components of the decaying and product charged leptons, is perfectly fine. The study is the first of its kind, catching a major role of the μ_i's, as well as the soft bilinear RPV parameters B_i's, in the LFV process in conjunction with the λ-type couplings.[3]

As advertised, our analysis here goes beyond that. Let us start by looking into the full mass eigenstate couplings of the truly physical charged leptons.

A. Charged scalar vertices

A charged lepton $\ell_i^\pm$ (or a generic $\chi_n^\pm$) couples to a charged scalar and a neutral fermion. From carefully expanding the Lagrangian, we have the vertices

$$g_2 \bar{\Psi}(\chi_{\bar{n}}^-)\left[\mathcal{N}^L_{\bar{n}mn}\frac{1-\gamma_5}{2}+\mathcal{N}^R_{\bar{n}mn}\frac{1+\gamma_5}{2}\right]\Psi(\chi_n^0)\phi_m^- + \text{H.c.}, \tag{3}$$

where $\frac{1}{2}(1 \mp \gamma_5)$ are the L- and R-handed projections and

$$\begin{aligned}\mathcal{N}^R_{\bar{n}mn} = {} & \boldsymbol{U}^*_{1\bar{n}}\boldsymbol{X}^*_{4n}\mathcal{D}^l_{2m} + \boldsymbol{U}^*_{1\bar{n}}\boldsymbol{X}^*_{(k+4)n}\mathcal{D}^l_{(k+2)m} + \frac{y_{e_k}}{g_2}\boldsymbol{U}^*_{2\bar{n}}\boldsymbol{X}^*_{(k+4)n}\mathcal{D}^l_{(k+5)m} + \frac{1}{\sqrt{2}}\boldsymbol{U}^*_{2\bar{n}}[\tan\theta_W \boldsymbol{X}^*_{1n} + \boldsymbol{X}^*_{2n}]\mathcal{D}^l_{2m} \\ & + \frac{1}{\sqrt{2}}\boldsymbol{U}^*_{(j+2)\bar{n}}[\tan\theta_W \boldsymbol{X}^*_{1n} + \boldsymbol{X}^*_{2n}]\mathcal{D}^l_{(j+2)m} - \frac{y_{e_j}}{g_2}\boldsymbol{U}^*_{(j+2)\bar{n}}\boldsymbol{X}^*_{4n}\mathcal{D}^l_{(j+5)m} - \frac{\lambda^*_{kjh}}{g_2}\boldsymbol{U}^*_{(j+2)\bar{n}}\boldsymbol{X}^*_{(k+4)n}\mathcal{D}^l_{(h+5)m},\end{aligned} \tag{4}$$

$$\begin{aligned}\mathcal{N}^L_{\bar{n}mn} = {} & -\boldsymbol{V}^*_{1\bar{n}}\boldsymbol{X}^*_{4n}\mathcal{D}^l_{2m} - \boldsymbol{V}^*_{1\bar{n}}\boldsymbol{X}^*_{(k+4)n}\mathcal{D}^l_{(k+2)m} + \frac{1}{\sqrt{2}}\boldsymbol{V}^*_{2\bar{n}}[-\tan\theta_W \boldsymbol{X}_{1n} + \boldsymbol{X}_{2n}]\mathcal{D}^l_{1m} - \sqrt{2}\tan\theta_W \boldsymbol{V}^*_{(j+2)\bar{n}}\boldsymbol{X}_{1n}\mathcal{D}^l_{(j+5)m} \\ & - \frac{y_{e_j}}{g_2}\boldsymbol{V}^*_{(j+2)\bar{n}}\boldsymbol{X}_{4n}\mathcal{D}^l_{(j+2)m} + \frac{y_{e_j}}{g_2}\boldsymbol{V}^*_{(j+2)\bar{n}}\boldsymbol{X}_{(j+4)n}\mathcal{D}^l_{2m} - \frac{\lambda_{khj}}{g_2}\boldsymbol{V}^*_{(j+2)\bar{n}}\boldsymbol{X}_{(k+4)n}\mathcal{D}^l_{(h+2)m},\end{aligned} \tag{5}$$

with $\bar{n}$ runs from 1 to 5, n from 1 to 7, and m from 1 to 8. $\boldsymbol{V}$ and $\boldsymbol{U}$ are unitary matrices used to diagonalize the charged fermion mass matrix, and $\boldsymbol{X}$ is the diagonalizing matrix of the neutral fermion mass matrix. $\mathcal{D}^l$ is the diagonalizing matrix of the charged scalar mass matrix [9]. We quote the corresponding terms $\mathcal{N}^R_{inm}$ and $\mathcal{N}^L_{inm}$ from an earlier formula in Ref. [13] for comparison:

$$\begin{aligned}\mathcal{N}^R_{inm} = {} & \frac{1}{\sqrt{2}}[\tan\theta_W \boldsymbol{X}^*_{1n} + \boldsymbol{X}^*_{2n}]\mathcal{D}^l_{(i+2)m} - \frac{y_{e_i}}{g_2}\boldsymbol{X}^*_{4n}\mathcal{D}^l_{(i+5)m} \\ & - \frac{\lambda^*_{kih}}{g_2}\boldsymbol{X}^*_{(k+4)n}\mathcal{D}^l_{(h+5)m}, \\ \mathcal{N}^L_{inm} = {} & -\sqrt{2}\tan\theta_W \boldsymbol{X}_{1n}\mathcal{D}^l_{(i+5)m} - \frac{y_{e_i}}{g_2}\boldsymbol{X}_{4n}\mathcal{D}^l_{(i+2)m} \\ & + \frac{y_{e_i}}{g_2}\boldsymbol{X}_{(k+4)n}\mathcal{D}^l_{2m} - \frac{\lambda_{khi}}{g_2}\boldsymbol{X}_{(k+4)n}\mathcal{D}^l_{(h+2)m}.\end{aligned} \tag{6}$$

One-loop diagrams formed by the pair of coupling vertices give rise to a class of contributions to the radiative decays we call neutralinolike, which obviously does include the ones with the physical neutralinos among the fermions running inside the loop. The new contributions come from the first five terms of Eq. (4) and first four terms of Eq. (5), which are not seen in Ref. [13]. These new terms involve Higgsinos and winos on the external legs and are easy to understand. For example, in $\mathcal{N}^R_{\bar{n}mn}$, the first term denotes the interaction with wino, neutral Higgsino, and charged Higgs. The second term is the interaction with wino, L-handed sleptons, and the neutrino flavor states, while the third term describes the interaction with charged Higgsino, neutrino, and R-handed sleptons. The last two terms denote the interactions with charged Higgsino, charged Higgs, and the bino and wino, respectively. The nonzero μ's do give the physical charged leptons some Higgsino or gaugino components.

B. Neutral scalar vertices

Next, we come to the charginolike contributions. Here we have to pair up neutral scalar vertices:

$$g_2 \bar{\Psi}(\chi_{\bar{n}}^-)\left[\mathcal{C}^L_{\bar{n}mn}\frac{1-\gamma_5}{2}+\mathcal{C}^R_{\bar{n}mn}\frac{1+\gamma_5}{2}\right]\Psi(\chi_n^-)\phi_m^0 + \text{H.c.}, \tag{7}$$

where

[3] See, however, studies on the $\mu_i^* \lambda'_{ijk}$ RPV contributions for similar processes in the quark sector [15]. In fact, the general relevancy of the kind of parameter combinations to flavor diagonal and off-diagonal dipole moments for fermions was first pointed out in Ref. [12].

$$\mathcal{C}^R_{\bar{n}mn} = \boldsymbol{U}^*_{1\bar{n}}\boldsymbol{V}_{2n}\frac{1}{\sqrt{2}}[\mathcal{D}^s_{1m} - i\mathcal{D}^s_{6m}] - \boldsymbol{U}^*_{2\bar{n}}\boldsymbol{V}_{1n}\frac{1}{\sqrt{2}}[\mathcal{D}^s_{2m} + i\mathcal{D}^s_{7m}] - \boldsymbol{U}^*_{(j+2)\bar{n}}\boldsymbol{V}_{1n}\frac{1}{\sqrt{2}}[\mathcal{D}^s_{(j+2)m} + i\mathcal{D}^s_{(j+7)m}]$$
$$+ \frac{y_{e_j}}{g_2}\boldsymbol{U}^*_{2\bar{n}}\boldsymbol{V}_{(j+2)n}\frac{1}{\sqrt{2}}[\mathcal{D}^{s*}_{(j+2)m} - i\mathcal{D}^{s*}_{(j+7)m}] - \frac{y_{e_j}}{g_2}\boldsymbol{U}^*_{(j+2)\bar{n}}\boldsymbol{V}_{(j+2)n}\frac{1}{\sqrt{2}}[\mathcal{D}^{s*}_{2m} - i\mathcal{D}^{s*}_{7m}]$$
$$- \frac{\lambda^*_{hjk}}{g_2}\boldsymbol{U}^*_{(j+2)\bar{n}}\boldsymbol{V}_{(k+2)n}\frac{1}{\sqrt{2}}[\mathcal{D}^{s*}_{(h+2)m} - i\mathcal{D}^{s*}_{(h+7)m}], \tag{8}$$

$$\mathcal{C}^L_{\bar{n}mn} = \boldsymbol{V}^*_{2\bar{n}}\boldsymbol{U}_{1n}\frac{1}{\sqrt{2}}[\mathcal{D}^{s*}_{1m} + i\mathcal{D}^{s*}_{6m}] - \boldsymbol{V}^*_{1\bar{n}}\boldsymbol{U}_{2n}\frac{1}{\sqrt{2}}[\mathcal{D}^{s*}_{2m} - i\mathcal{D}^{s*}_{7m}] - \boldsymbol{V}^*_{1\bar{n}}\boldsymbol{U}_{(j+2)n}\frac{1}{\sqrt{2}}[\mathcal{D}^{s*}_{(j+2)m} - i\mathcal{D}^{s*}_{(j+7)m}]$$
$$+ \frac{y_{e_j}}{g_2}\boldsymbol{V}^*_{(j+2)\bar{n}}\boldsymbol{U}_{2n}\frac{1}{\sqrt{2}}[\mathcal{D}^s_{(j+2)m} + i\mathcal{D}^s_{(j+7)m}] - \frac{y_{e_j}}{g_2}\boldsymbol{V}^*_{(j+2)\bar{n}}\boldsymbol{U}_{(j+2)n}\frac{1}{\sqrt{2}}[\mathcal{D}^s_{2m} + i\mathcal{D}^s_{7m}]$$
$$+ \frac{\lambda_{khj}}{g_2}\boldsymbol{V}^*_{(j+2)\bar{n}}\boldsymbol{U}_{(k+2)n}\frac{1}{\sqrt{2}}[\mathcal{D}^s_{(h+2)m} + i\mathcal{D}^s_{(h+7)m}], \tag{9}$$

with n and $\bar{n}$ run from 1 to 5 and m from 1 to 10. $\mathcal{D}^s$ is the diagonalizing matrix of the neutral scalar mass matrix [9]. Note that $\mathcal{C}^L_{\bar{n}mn}$ is equal to $\mathcal{C}^{R^*}_{nm\bar{n}}$ by definition. These are to replace $\mathcal{C}^L_{\bar{n}mn}$ and $\mathcal{C}^{R^*}_{nm\bar{n}}$ of Ref. [13][4]

$$\mathcal{C}^R_{inm} = \boldsymbol{V}_{1n}\frac{1}{\sqrt{2}}[\mathcal{D}^s_{(i+2)m} + i\mathcal{D}^s_{(i+7)m}]$$
$$- \frac{y_{e_i}}{g_2}\boldsymbol{V}_{(i+2)n}\frac{1}{\sqrt{2}}[\mathcal{D}^s_{2m} - i\mathcal{D}^s_{7m}]$$
$$- \frac{\lambda^*_{hik}}{g_2}\boldsymbol{V}_{(k+2)n}\frac{1}{\sqrt{2}}[\mathcal{D}^s_{(h+2)m} - i\mathcal{D}^s_{(j+7)m}],$$
$$\mathcal{C}^L_{inm} = \frac{y_{e_i}}{g_2}\boldsymbol{U}_{2n}\frac{1}{\sqrt{2}}[\mathcal{D}^s_{(i+2)m} + i\mathcal{D}^s_{(i+7)m}] \tag{10}$$
$$- \frac{y_{e_i}}{g_2}\boldsymbol{U}_{(j+2)n}\frac{1}{\sqrt{2}}[\mathcal{D}^s_{2m} + i\mathcal{D}^s_{7m}]$$
$$+ \frac{\lambda_{khi}}{g_2}\boldsymbol{U}_{(k+2)n}\frac{1}{\sqrt{2}}[\mathcal{D}^s_{(h+2)m} + i\mathcal{D}^s_{(h+7)m}].$$

Note that $\mathcal{D}^s$ is actually real, though we are using $\mathcal{D}^{s*}$ notation as if it is not. This is just a convention for tracing the LFV structure of the various contributions in our analytical discussions below. Here, in fact, the real difference between the $\mathcal{D}^{s*}$ and $\mathcal{D}^s$ terms is given explicitly by the different signs between the corresponding scalar and pseudoscalar parts. Note that the y_{e_i} terms in the above expressions can be written together with the λ terms using the $\lambda_{\alpha\beta k}$ notation and the identification of y_{e_i} as λ_{0ii}. This common structure between $\hat{L}_0$ and the $\hat{L}_i$'s is very useful in our discussions below.

[4]Recall that in the latter case, one distinguishes the "external" charged lepton, approximated by an $l^{\pm}$, from an "internal" charged fermion mass eigenstate.

C. The decay amplitude

In applying the above interactions to the process $\ell^-_j(p) \to \ell^-_i\gamma(q)$, we can write the amplitude as

$$T = e\epsilon^{*\alpha}\bar{u}_i(p-q)\Big[m_{\ell_j}i\sigma_{\alpha\beta}q^\beta\Big(A^L_2\frac{1-\gamma_5}{2} + A^R_2\frac{1+\gamma_5}{2}\Big)\Big]u_j(p), \tag{11}$$

where $\epsilon^* = \epsilon^*(q)$ is the polarization four-vector of the outgoing photon. The decay rate is then simply given by

$$\Gamma(\ell^-_j \to \ell^-_i\gamma) = \frac{\alpha_{\rm em}}{4}m^5_{\ell_j}(|A^L_2|^2 + |A^R_2|^2). \tag{12}$$

It is straightforward to calculate the contributions from one-loop diagrams with the effective interactions of Eqs. (3) and (7). The result for A^L_2 ($A^R_2 = A^L_2|_{L\leftrightarrow R}$) is given by

$$A^L_2 = \frac{\alpha_{\rm em}}{8\pi\sin^2\theta_W}\frac{1}{M^2_{\tilde{\ell}_m}}\Big[\mathcal{N}^L_{(i+2)mn}\mathcal{N}^{L^*}_{(j+2)mn}F_2\Big(\frac{M^2_{\chi^0_n}}{M^2_{\tilde{\ell}_m}}\Big)$$
$$+ \mathcal{N}^R_{(i+2)mn}\mathcal{N}^{R^*}_{(j+2)mn}\frac{m_{\ell_i}}{m_{\ell_j}}F_2\Big(\frac{M^2_{\chi^0_n}}{M^2_{\tilde{\ell}_m}}\Big)$$
$$+ \mathcal{N}^L_{(i+2)mn}\mathcal{N}^{R^*}_{(j+2)mn}\frac{M_{\chi^0_n}}{m_{\ell_j}}F_3\Big(\frac{M^2_{\chi^0_n}}{M^2_{\tilde{\ell}_m}}\Big)\Big]$$
$$- \frac{\alpha_{\rm em}}{8\pi\sin^2\theta_W}\frac{1}{M^2_{S_m}}\Big[\mathcal{C}^L_{(i+2)mn}\mathcal{C}^{L^*}_{(j+2)mn}F_5\Big(\frac{M^2_{\chi^-_n}}{M^2_{S_m}}\Big)$$
$$+ \mathcal{C}^R_{(i+2)mn}\mathcal{C}^{R^*}_{(j+2)mn}\frac{m_{\ell_i}}{m_{\ell_j}}F_5\Big(\frac{M^2_{\chi^-_n}}{M^2_{S_m}}\Big)$$
$$+ \mathcal{C}^L_{(i+2)mn}\mathcal{C}^{R^*}_{(j+2)mn}\frac{M_{\chi^-_n}}{m_{\ell_j}}F_6\Big(\frac{M^2_{\chi^-_n}}{M^2_{S_m}}\Big)\Big], \tag{13}$$

where

$$F_2(x) = \frac{1}{6(1-x)^4}(1 - 6x + 3x^2 + 2x^3 - 6x^2 \ln x),$$

$$F_3(x) = \frac{1}{(1-x)^3}(1 - x^2 + 2x \ln x),$$

$$F_5(x) = \frac{1}{6(1-x)^4}(2 + 3x - 6x^2 + x^3 + 6x \ln x),$$

$$F_6(x) = \frac{1}{(1-x)^3}(-3 + 4x - x^2 - 2 \ln x),$$

with summations over all physical fermion and scalar mass eigenstates as represented by the n and m indices assumed.

The processes we discuss here violate lepton flavor while conserving the lepton number. Before going into the analysis, it is instructive to introduce the lepton-flavor numbers L_e, L_μ, and L_τ to the superfields as one does to their corresponding components in the SM. The RPV parameters bear violations of the lepton-flavor numbers. It is obvious that in order to have a contribution to $\ell_j^- \to \ell_i^- \gamma$, a term must reduce L_j and increase L_i by exactly one unit while leaving the rest unchanged. For instance, $\mu_1^* \mu_2$ means increasing a L_e and reducing a L_μ while leaving L_τ unchanged. This simple but useful rule serves as a countercheck of individual contributions discussed below.

IV. NUMERICAL RESULTS AND DISCUSSIONS

In this section, we present the results we obtained by a careful numerical implementation of our $\mu \to e\gamma$, $\tau \to e\gamma$, and $\tau \to \mu\gamma$ formula with explicit numerical diagonalization of all the mass matrices involved. We isolate various major contributions by singling out each of the corresponding RPV parameter combinations as only nonvanishing one at a time. The soft SUSY breaking contributions to R-parity conserving slepton mixings are set to zero (i.e. $\tilde{m}_L^2$, $\tilde{m}_E^2$, and A^E are set to be diagonal). A basic set of typical values chosen for the input parameters are given in Table I. We used this set of inputs unless otherwise specified in the results below. A summary of bounds on various combinations of two R-parity violating parameters is shown in Table II. Neutrino mass bounds are also put onto the plots. We perform numerical calculation of the neutrino mass contributions from various parameters involved based on formulas from Ref. [21]. The bounds are obtained naively by requiring that individual neutrino mass terms obtained be less than the sub-eV level. Note that each of these bounds has different dependence on the background model parameters and are also typically different from the leptonic decay contribution term plotted. Hence, the comparison has only a simple illustrative value. A more comprehensive cross analysis is, however, considered not appropriate without taking further assumption on some of the parameters involved. At the end, we also show some of the effects of varying these input parameters.

TABLE I. Basic input SUSY parameters for the numerical results presented. These values are adopted unless otherwise specified.

M_1 (GeV)	M_2 (GeV)	μ_0 (GeV)	$\tan\beta$
100	200	135	40
$\tilde{m}_L^2$ (10^4 GeV^2)	$\tilde{m}_E^2$ (10^4 GeV^2)	A_e (GeV)	
diag{2, 1, 1, 1}	diag{1, 1, 1}	100	

A. The $|\mu^* \lambda|$ or $|B^* \lambda|$ contributions

We first look at the contributions with a $(\mu^* \lambda)$ or $(\mu \lambda^*)$ structure. The dominant terms do not involve the Higgsino or wino component of the decaying or the product charged leptons. They come from the third term of $\mathcal{C}^R_{\bar{n}mn}$ and the only one λ-coupling vertex of $\mathcal{C}^L_{\bar{n}mn}$, corresponding to the diagrams with the chirality flip on the internal fermion line. Indeed, the role of the μ_i's come in through the internal fermion line, as discussed in good detail in Ref. [13]. Take A_2^L, for example, the dominating term comes from $\mathcal{C}^L_{\bar{n}'mn}\mathcal{C}^{R^*}_{\bar{n}mn}$, where $\bar{n}' < \bar{n}$. We then have the real scalar part of the contribution, for example, proportional to

$$\sum_{n=1}^{5}\sum_{m=1}^{5} \boldsymbol{U}_{(j+2)\bar{n}} \boldsymbol{V}^*_{(j'+2)\bar{n}'} \boldsymbol{V}^*_{1n} M_{\chi_n^-} \boldsymbol{U}_{(k+2)n} F_6\left(\frac{M^2_{\chi_n^-}}{M^2_{S_m}}\right) \times \mathcal{D}^{s*}_{(j+2)m} \mathcal{D}^{s}_{(h+2)m} \frac{\lambda_{khj'}}{g_2}. \tag{14}$$

In the $\mu \to e\gamma$ case, we have $\bar{n}' = 3$ and $\bar{n} = 4$ and then use the relation $\boldsymbol{U}_{(j+2)\bar{n}} \sim \delta_{(j+2),\bar{n}}$ and $\boldsymbol{V}^*_{(j'+2)\bar{n}'} \sim \delta_{(j'+2),\bar{n}'}$. The expression (14) can be given by

$$\sum_{n=1}^{5}\sum_{m=1}^{5} \boldsymbol{V}^*_{1n} M_{\chi_n^-} \boldsymbol{U}_{(k+2)n} F_6\left(\frac{M^2_{\chi_n^-}}{M^2_{S_m}}\right) \mathcal{D}^{s*}_{4m} \mathcal{D}^{s}_{(h+2)m} \frac{\lambda_{kh1}}{g_2}. \tag{15}$$

If the loop function F_6 could be factored out from the double summation, we would have a $\boldsymbol{V}^*_{1n} M_{\chi_n^-} \boldsymbol{U}_{(k+2)n}$ summation over fermions and a $\mathcal{D}^{s*}_{4m}\mathcal{D}^{s}_{(h+2)m}$ summation over (real) scalars. Taking $h = 2$ in the above expression (15), we have the two dominating chargino contributions, the $n = 1$ and 2 parts, given approximately by

$$\boldsymbol{V}^*_{1n} \mu_k^* R_{R_{2n}} \frac{\lambda_{k21}}{g_2} F_6\left(\frac{M^2_{\chi_n^-}}{M^2_{S_m}}\right), \tag{16}$$

where R_R is a 2×2 matrix with order 1 matrix elements (see Ref. [9] for details.) The expected combination $\mu_k^* \lambda_{k21}$ comes up, with $k = 1$ and 3 admissible. The same situation goes for the $\mathcal{C}^R_{3mn}\mathcal{C}^{L^*}_{4mn}$ part of A_2^R, with the combination $\mu_k \lambda^*_{k12}$ ($k = 2$ and 3 admissible here) instead.

Terms involving the Higgsino and wino components of the decaying and product charged leptons are expected to be proportional to $\boldsymbol{U}_{a\bar{n}}$ or $\boldsymbol{V}_{a\bar{n}}$ for $a = 1$ or 2, with [9]

$$\boldsymbol{U}_{a(i+2)} \propto \mu_i, \qquad \boldsymbol{V}_{a(i+2)} \propto \mu_i m_i. \tag{17}$$

In the case of the $\mu \to e\gamma$, if we focus on the μ_3^* and λ_{321} parameter combination, the new contributions of $\mathcal{N}^{L,R}_{3mn}$, $\mathcal{N}^{L,R}_{4mn}$, $\mathcal{C}^{L,R}_{3mn}$, and $\mathcal{C}^{L,R}_{4mn}$ do not contribute to the Br($\mu \to e\gamma$), since they are only proportional to the μ_1 or μ_2, not μ_3. Likewise, the $\mu_3\lambda^*_{312}$ also does not have a new contribution to Br($\mu \to e\gamma$). For the same reason, the contributions of $\mu_1\lambda^*_{123}$, $\mu_1^*\lambda_{132}$, $\mu_2\lambda^*_{213}$, $\mu_2^*\lambda_{231}$, and all $B^*\lambda$ and $B\lambda^*$ type combinations to the branching ratio of leptonic radiative decays are still essentially the same as the results obtained by neglecting the wino and Higgino components of the decaying and product charged leptons.

There are, however, new contributions that come from the charginolike loop diagrams with the chirality flip on the external fermion line. They are the product of the fourth term and the λ-coupling term of $\mathcal{C}^R_{\bar{n}mn}$. There are two types of diagrams. The first type comes from $\mathcal{C}^R_{\bar{n}'mn}\mathcal{C}^{R^*}_{\bar{n}mn}$, where $\bar{n}' < \bar{n}$, with a λ coupling in the $\mathcal{C}^{R^*}_{\bar{n}mn}$ and a Yukawa coupling in the $\mathcal{C}^R_{\bar{n}'mn}$. It is given by

$$m_\ell \sum_{n=1}^{5}\sum_{m=1}^{5} \boldsymbol{U}^*_{2\bar{n}'}\boldsymbol{U}_{(j+2)\bar{n}}\boldsymbol{V}_{(j'+2)n}\boldsymbol{V}^*_{(k+2)n} F_5\left(\frac{M^2_{\chi^-_n}}{M^2_{S_m}}\right) \times \mathcal{D}^{s*}_{(j'+2)m}\mathcal{D}^s_{(h+2)m}\frac{-\lambda_{hjk}}{g_2}\frac{y_{e_{j'}}}{g_2}, \tag{18}$$

requiring further $h = j'$ and $k = j'$. Note that all off-diagonal matrix elements of the form $\boldsymbol{V}_{(k+2)n}$ are very small, those RPV ones ($n = 1$ or 2), in particular, contain a y_{e_k} suppression [9]. A similar situation goes with the scalar sum $\mathcal{D}^{s*}_{(j'+2)m}\mathcal{D}^s_{(h+2)m} = \delta_{j'h}$ by unitarity. m_ℓ stands for the mass of the decaying lepton. There is a factor of $y_{e_{j'}}$ suppression in the expression (18). The electroweak state Feynman diagram of this expression is in Fig. 1. Note the Higgsino component of an external line illustrated.

In the case of $\tau \to \mu\gamma$, we have $\bar{n}' = 4$ and $\bar{n} = 5$. After we take $j' = h = k = 2$ in the expression (18) and use the relation $\boldsymbol{U}_{(j+2)\bar{n}} \sim \delta_{(j+2),\bar{n}}$ and $\boldsymbol{U}^*_{2(i+2)} \propto \mu_i^*$, the expression (18) can be given approximately by

$$m_\tau \mu_2^* \frac{\lambda_{232}}{g_2}\frac{y_{e_2}}{g_2} F_5\left(\frac{M^2_{\chi^-_n}}{M^2_{S_m}}\right). \tag{19}$$

The expected $\mu_2^*\lambda_{232}$ comes out with a factor of y_{e_2} (muon Yukawa coupling) suppression. The same situation goes for the case of the $\mu \to e\gamma$ and $\tau \to e\gamma$, corresponding to the combination of $\mu_1^*\lambda_{121}$ and $\mu_1^*\lambda_{131}$, respectively, with a y_{e_1} suppression.

Likewise, the second type comes from $\mathcal{C}^R_{\bar{n}'mn}\mathcal{C}^{R^*}_{\bar{n}mn}$, where $\bar{n}' < \bar{n}$, with a λ coupling in the $\mathcal{C}^R_{\bar{n}'mn}$ and a Yukawa coupling in the $\mathcal{C}^{R^*}_{\bar{n}mn}$. It is given by

$$m_\ell \sum_{n=1}^{5}\sum_{m=1}^{5} \boldsymbol{U}_{2\bar{n}}\boldsymbol{U}^*_{(j'+2)\bar{n}'}\boldsymbol{V}^*_{(j+2)n}\boldsymbol{V}_{(k+2)n} F_5\left(\frac{M^2_{\chi^-_n}}{M^2_{S_m}}\right) \times \mathcal{D}^s_{(j+2)m}\mathcal{D}^{s*}_{(h+2)m}\frac{-\lambda^*_{hj'k}}{g_2}\frac{y_{e_j}}{g_2}. \tag{20}$$

The electroweak state Feynman diagram for this case is in Fig. 2. In the case of $\mu \to e\gamma$, we have $\bar{n}' = 3$ and $\bar{n} = 4$. After taking $j = h = k = 2$ and using the relation men-

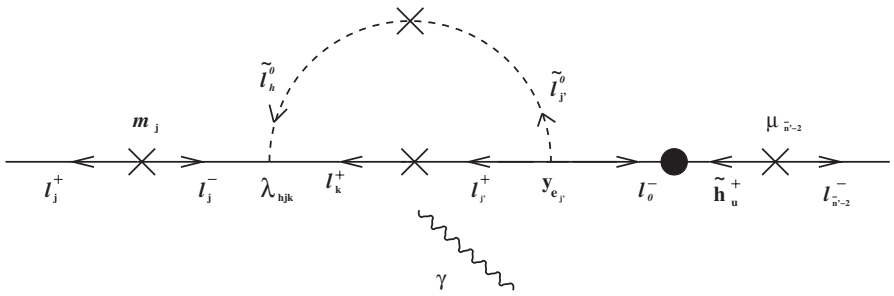

FIG. 1. Diagram with chirality flip on the external line, which has larger Yukawa suppression.

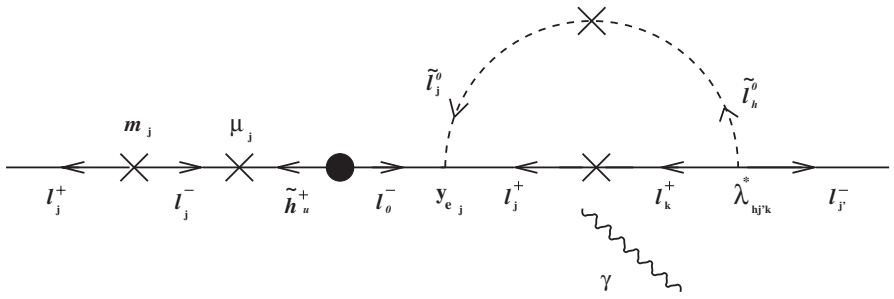

FIG. 2. Diagram with chirality flip on the external line, which has smaller Yukawa suppression.

tioned above, the expected $\mu_2\lambda^*_{212}$ would come out, with a factor of muon Yukawa. The same situation goes for the case of the $\tau \to e\gamma$, and $\tau \to \mu\gamma$, corresponding to the combination of $\mu_3\lambda^*_{313}$ and $\mu_3\lambda^*_{323}$, respectively, with a tau Yukawa. Compared with the first type, the second one does have larger contributions, since the former have the stronger Yukawa suppression. This result is confirmed by our exact numerical calculation and could be understood easily through Figs. 1 and 2, where the relevant illustrative electroweak state one-loop diagrams are given. Because these two types of contributions involve leptonic Yukawa couplings, they have $\frac{1}{\cos\beta}$ dependence. However, they are not the dominant contributions, so the $\mu^*\lambda$ or $\mu\lambda^*$ type contributions are still insensitive to the $\tan\beta$.

We plot contours of the resulting branching ratio as a function of (real) μ_2 and λ_{212}, μ_3 and λ_{323}, and μ_3 and λ_{313} in Figs. 3–5, respectively. The present experimental limit is also shown and the allowed region at 90% C.L. is shaded. The 90% C.L. upper limit on $|\mu^*_k\lambda_{k21}|$ or $|\mu_k\lambda^*_{k12}|$ (normalized by $|\mu_0| = 135$ GeV) is given by

$$\frac{|\mu^*_3\lambda_{321}|}{|\mu_0|}, \quad \frac{|\mu^*_1\lambda_{121}|}{|\mu_0|}, \quad \frac{|\mu_3\lambda^*_{312}|}{|\mu_0|}, \quad \frac{|\mu_2\lambda^*_{212}|}{|\mu_0|} < 2.1 \times 10^{-7}. \tag{21}$$

Likewise, the 90% C.L. upper limit on $|\mu^*_k\lambda_{k32}|$ or $|\mu_k\lambda^*_{k23}|$ (normalized by $|\mu_0| = 135$ GeV) is given by

$$\frac{|\mu^*_2\lambda_{232}|}{|\mu_0|}, \quad \frac{|\mu^*_1\lambda_{132}|}{|\mu_0|}, \quad \frac{|\mu_3\lambda^*_{323}|}{|\mu_0|}, \quad \frac{|\mu_1\lambda^*_{123}|}{|\mu_0|} < 7.0 \times 10^{-4}. \tag{22}$$

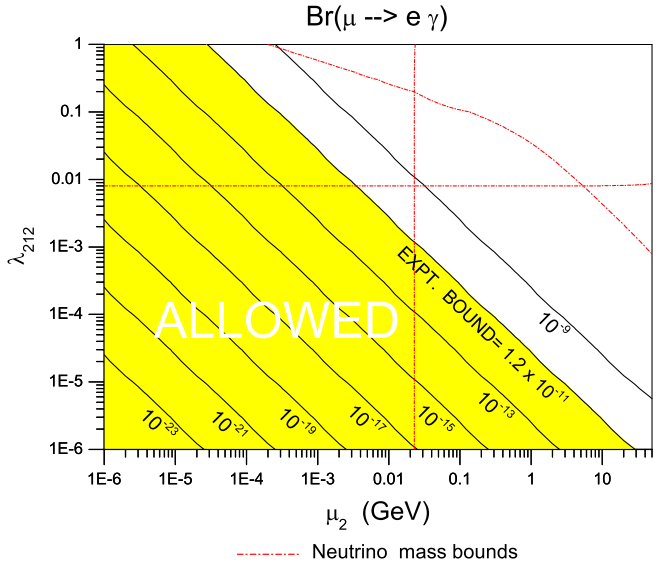

FIG. 3 (color online). Contours of $B(\mu \to e\gamma)$ in the (real) plane of (μ_2, λ_{212}). The 90% C.L. allowed region is shaded. The dash-dotted (red) lines are sub-eV neutrino mass bounds.

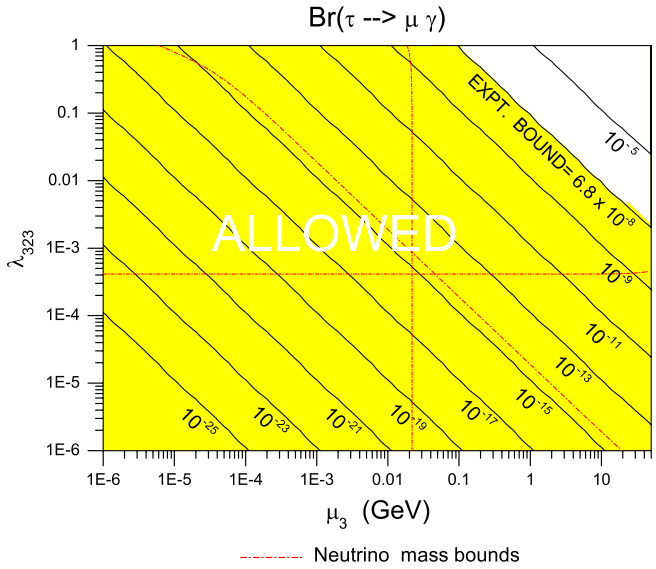

FIG. 4 (color online). Contours of $B(\tau \to \mu\gamma)$ in the (real) plane of (μ_3, λ_{323}). The 90% C.L. allowed region is shaded. The dash-dotted (red) lines are sub-eV neutrino mass bounds.

The 90% C.L. upper limit on $|\mu^*_k\lambda_{k31}|$ or $|\mu_k\lambda^*_{k13}|$ (normalized by $|\mu_0| = 135$ GeV) is given by

$$\frac{|\mu^*_2\lambda_{231}|}{|\mu_0|}, \quad \frac{|\mu^*_1\lambda_{131}|}{|\mu_0|}, \quad \frac{|\mu_3\lambda^*_{313}|}{|\mu_0|}, \quad \frac{|\mu_2\lambda^*_{213}|}{|\mu_0|} < 8.5 \times 10^{-4}. \tag{23}$$

For the $B\lambda^*$ structure, one of the contributions is from the chirality flip inside the loop. In A^L_2, this term comes from the λ coupling term of $\mathcal{C}^L_{\vec{n}'mn}$ and the fifth term of

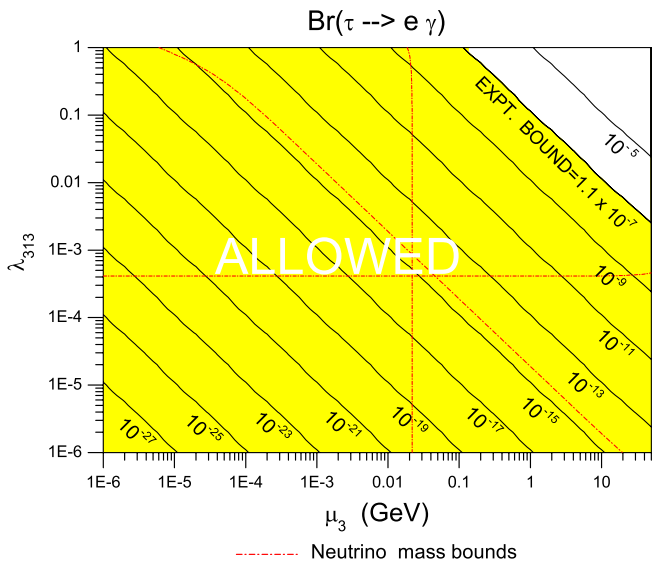

FIG. 5 (color online). Contours of $B(\tau \to e\gamma)$ in the (real) plane of (μ_3, λ_{313}). The 90% C.L. allowed region is shaded. The dash-dotted (red) lines are sub-eV neutrino mass bounds.

$\mathcal{C}^R_{\bar{n}mn}$, where $\bar{n}' < \bar{n}$. We then have the expression

$$\sum_m{}' \sum_{n=1}^{5} \boldsymbol{V}^*_{(j'+2)\bar{n}'} \boldsymbol{U}_{(j+2)\bar{n}} \boldsymbol{V}^*_{(j+2)n} M_{\chi_n^-} \boldsymbol{U}_{(k+2)n} F_6\left(\frac{M^2_{\chi_n^-}}{M^2_{S_m}}\right) \cdot [\mathcal{D}^s_{2m} + i\mathcal{D}^s_{7m}][\mathcal{D}^s_{(h+2)m} + i\mathcal{D}^s_{(h+7)m}] \frac{y_{e_j}}{g_2} \frac{-\lambda_{hkj'}}{g_2}, \tag{24}$$

where the $\sum_m{}'$ notation means the unphysical Goldstone mode is omitted. In the case of $\mu \to e\gamma$, we have $\bar{n}' = 3$ and $\bar{n} = 4$. Using $\boldsymbol{V}^*_{(j'+2)\bar{n}'} \sim \delta_{(j'+2)\bar{n}'}$ and $\boldsymbol{U}_{(j+2)\bar{n}} \sim \delta_{(j+2)\bar{n}}$ and taking $k = 2$, we then have the expression

$$\sum_m{}' \sum_{n=1}^{5} \boldsymbol{V}^*_{4n} M_{\chi_n^-} \boldsymbol{U}_{4n} F_6\left(\frac{M^2_{\chi_n^-}}{M^2_{S_m}}\right)[\mathcal{D}^s_{2m} + i\mathcal{D}^s_{7m}] \times [\mathcal{D}^s_{(h+2)m} + i\mathcal{D}^s_{(h+7)m}] \frac{y_{e_2}}{g_2} \frac{-\lambda_{h21}}{g_2}. \tag{25}$$

The fermionic sum suggests a major contribution from $n = 4$, i.e. the muon itself with the m_μ dependence. However, this contribution then has two factors of ''muon Yukawa'' (y_{e_2}) suppression. The scalar sum gives a contribution proportional to $B^*_{j'} \tan\beta$. The expected combination $B^*_h \lambda_{h21}$ comes up with an explicit $\tan\beta$ dependence. The other contribution having similar strength to the one in expression (24) discussed above is from the chirality flip on the external muon line. In A^L_2, this term comes from the λ coupling term of $\mathcal{C}^L_{\bar{n}'mn}$ and the fifth term of $\mathcal{C}^L_{\bar{n}mn}$, where $\bar{n}' < \bar{n}$. We then have the contribution proportional to

$$m_\ell \sum_{n=1}^{5} \sum_{m=1}^{5} \boldsymbol{V}_{(j+2)\bar{n}} \boldsymbol{V}^*_{(j'+2)\bar{n}'} \boldsymbol{U}^*_{(j+2)n} \boldsymbol{U}_{(k+2)n} F_5\left(\frac{M^2_{\chi_n^-}}{M^2_{S_m}}\right) \times \mathcal{D}^s_{(h+2)m} \mathcal{D}^{s*}_{2m} \frac{-\lambda_{hkj'}}{g_2} \frac{-y_{e_j}}{g_2}. \tag{26}$$

In the case of $\mu \to e\gamma$, we have $\bar{n}' = 3$ and $\bar{n} = 4$. Using $\boldsymbol{V}_{(j+2)\bar{n}} \sim \delta_{(j+2),\bar{n}}$ and $\boldsymbol{V}^*_{(j'+2)\bar{n}'} \sim \delta_{(j'+2)\bar{n}'}$ and taking $k = 2$, we have the expression

$$m_\mu \sum_{n=1}^{5} \sum_{m=1}^{5} \boldsymbol{U}^*_{4n} \boldsymbol{U}_{4n} F_5\left(\frac{M^2_{\chi_n^-}}{M^2_{S_m}}\right) \mathcal{D}^s_{(h+2)m} \mathcal{D}^{s*}_{2m} \frac{-\lambda_{h21}}{g_2} \frac{-y_{e_2}}{g_2}, \tag{27}$$

where we have $h = 3$ or 1. The scalar sum gives the dominating contribution proportional to B^*_h. The expected combination $B^*_h \lambda_{h21}$ comes up. The 90% C.L. upper limit on $|B^*_k \lambda_{k21}|$ or $|B_k \lambda^*_{k12}|$ (normalized by $|\mu_0| = 135$ GeV) is given by

$$\frac{|B^*_3 \lambda_{321}|}{|\mu_0|^2}, \quad \frac{|B^*_1 \lambda_{121}|}{|\mu_0|^2}, \quad \frac{|B_3 \lambda^*_{312}|}{|\mu_0|^2}, \quad \frac{|B_2 \lambda^*_{212}|}{|\mu_0|^2} < 1.3 \times 10^{-4}. \tag{28}$$

Likewise, the 90% C.L. upper limit on $|B^*_k \lambda_{k32}|$ or $|B_k \lambda^*_{k23}|$ (normalized by $|\mu_0| = 135$ GeV) is given by

$$\frac{|B^*_2 \lambda_{232}|}{|\mu_0|^2}, \quad \frac{|B^*_1 \lambda_{132}|}{|\mu_0|^2}, \quad \frac{|B_3 \lambda^*_{323}|}{|\mu_0|^2}, \quad \frac{|B_1 \lambda^*_{123}|}{|\mu_0|^2} < 1.4 \times 10^{-3}. \tag{29}$$

The 90% C.L. upper limit on $|B^*_k \lambda_{k31}|$ or $|B_k \lambda^*_{k13}|$ (normalized by $|\mu_0| = 135$ GeV) is given by

$$\frac{|B^*_2 \lambda_{231}|}{|\mu_0|^2}, \quad \frac{|B^*_1 \lambda_{131}|}{|\mu_0|^2}, \quad \frac{|B_3 \lambda^*_{313}|}{|\mu_0|^2}, \quad \frac{|B_2 \lambda^*_{213}|}{|\mu_0|^2} < 1.9 \times 10^{-3}. \tag{30}$$

B. The $|B^*\mu|$ contributions

Next, we will discuss the $B^*\mu$ and $B\mu^*$ type combinations. The dominant terms come from two types of diagrams with the chirality flip inside the loop. One of them comes from the third term of $\mathcal{C}^R_{\bar{n}mn}$ and the fifth term of $\mathcal{C}^L_{\bar{n}mn}$. In A^R_2, this term comes from $\mathcal{C}^R_{\bar{n}'mn} \mathcal{C}^{L^*}_{\bar{n}mn}$, where $\bar{n}' < \bar{n}$. We then have the real scalar part of the contribution proportional to

$$\sum_{n=1}^{5} \sum_{m=1}^{5} \boldsymbol{U}^*_{(j'+2)\bar{n}'} \boldsymbol{V}_{(j+2)\bar{n}} \boldsymbol{V}_{1n} M_{\chi_n^-} \boldsymbol{U}^*_{(j+2)n} F_6\left(\frac{M^2_{\chi_n^-}}{M^2_{S_m}}\right) \times \mathcal{D}^s_{(j'+2)m} \mathcal{D}^{s*}_{2m} \frac{y_{e_j}}{g_2}. \tag{31}$$

The relevant electroweak state Feynman diagram is then in Fig. 6. With only $l^\pm_i$ on the external legs, it obviously involves no Higgsino or wino component there. The dominating part with the charginos ($n = 1$ and 2) gives a μ_j dependence through $\boldsymbol{U}^*_{(j+2)n}$. The scalar sum gives the contribution proportional to $B^*_{j'} \tan\beta$. The expected combination $B^*_{j'} \mu_j$ comes up with an explicit $\tan\beta$ dependence. Similarly, in A^L_2, this term comes from $\mathcal{C}^L_{\bar{n}'mn} \mathcal{C}^{R^*}_{\bar{n}mn}$, again $\bar{n}' < \bar{n}$. It is given by

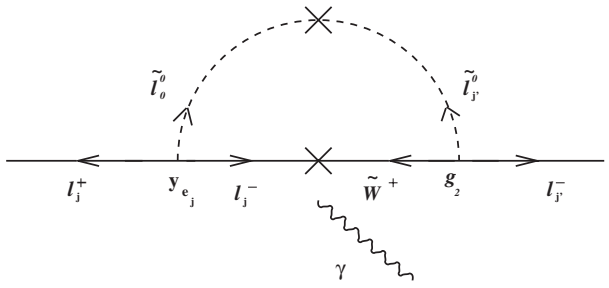

FIG. 6. The charginolike loop diagram contributes to the leptonic radiative decay due to $B^*_{j'} \mu_j$ combination.

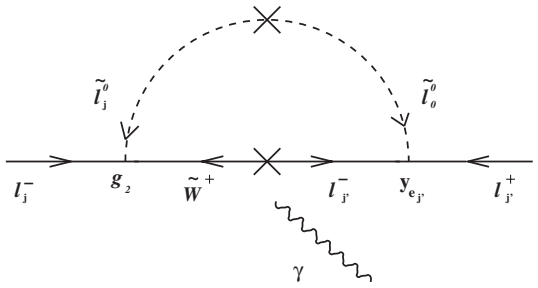

FIG. 7. The charginolike loop diagram contributes to the leptonic radiative decay due to $\mu^*_{j'}B_j$ combination.

$$\sum_{n=1}^{5}\sum_{m=1}^{5} \boldsymbol{V}^*_{(j'+2)\bar{n}'}\boldsymbol{U}_{(j+2)\bar{n}}\boldsymbol{U}_{(j'+2)n}M_{\chi^-_n}\boldsymbol{V}^*_{1n}F_6\left(\frac{M^2_{\chi^-_n}}{M^2_{S_m}}\right) \times \mathcal{D}^s_{2m}\mathcal{D}^{s*}_{(j+2)m}\frac{y_{e_{j'}}}{g_2}. \quad (32)$$

The expected combination $\mu^*_{j'}B_j$ comes up (see Fig. 7).

The other type of contribution comes from the second term of $\mathcal{C}^R_{\bar{n}mn}$ and the fourth term of $\mathcal{C}^L_{\bar{n}mn}$, which is a new contribution not considered in Ref. [13]. It does have a sizable contribution in some RPV parameter space regions. In A^R_2, this term comes from $\mathcal{C}^R_{\bar{n}'mn}\mathcal{C}^{L^*}_{\bar{n}mn}$. We then have the contribution proportional to

$$\sum_{n=1}^{5}\sum_{m=1}^{5} -\boldsymbol{U}^*_{2\bar{n}'}\boldsymbol{V}_{(j+2)\bar{n}}\boldsymbol{V}_{1n}M_{\chi^-_n}\boldsymbol{U}^*_{2n}F_6\left(\frac{M^2_{\chi^-_n}}{M^2_{S_m}}\right) \times \mathcal{D}^s_{2m}\mathcal{D}^{s*}_{(j+2)m}\frac{y_{e_j}}{g_2}. \quad (33)$$

We expect a $B_j\tan\beta$ from the scalar mixing part, and a $\mu^*_{\bar{n}'-2}$ from $\boldsymbol{U}^*_{2\bar{n}'}$. In A^L_2, this term comes from $\mathcal{C}^L_{\bar{n}'mn}\mathcal{C}^{R^*}_{\bar{n}mn}$. It is given by

$$\sum_{n=1}^{5}\sum_{m=1}^{5} -\boldsymbol{V}^*_{(j'+2)\bar{n}'}\boldsymbol{U}_{2\bar{n}}\boldsymbol{U}_{2n}M_{\chi^-_n}\boldsymbol{V}^*_{1n}F_6\left(\frac{M^2_{\chi^-_n}}{M^2_{S_m}}\right) \times \mathcal{D}^s_{(j'+2)m}\mathcal{D}^{s*}_{2m}\frac{y_{e_{j'}}}{g_2}. \quad (34)$$

Again, we expect a $B^*_{j'}\tan\beta$ from the scalar mixing part, and a $\mu_{\bar{n}-2}$ from the $\boldsymbol{U}_{2\bar{n}}$. The relevant electroweak state Feynman diagrams for the cases are given in Figs. 8 and 9, respectively. They clearly illustrate the role of the Higgsino component on an external line.

Taking the $\mu \to e\gamma$, for example, we have $\bar{n}' = 3$ and $\bar{n} = 4$. The expression (31) would become

$$\sum_{n=1}^{5}\sum_{m=1}^{5} \boldsymbol{V}_{1n}M_{\chi^-_n}\boldsymbol{U}^*_{4n}F_6\left(\frac{M^2_{\chi^-_n}}{M^2_{S_m}}\right)\mathcal{D}^s_{3m}\mathcal{D}^{s*}_{2m}\frac{y_{e_2}}{g_2}, \quad (35)$$

where we used the relation $\boldsymbol{U}^*_{(j'+2)3} \sim \delta_{j',1}$ and $\boldsymbol{V}_{(j+2)4} \sim \delta_{j,2}$. As mentioned above, the expected $B^*_1\mu_2$ combination comes up. It clearly has a muon Yukawa suppression. Likewise, the expression (32) becomes

$$\sum_{n=1}^{5}\sum_{m=1}^{5} \boldsymbol{V}^*_{1n}M_{\chi^-_n}\boldsymbol{U}_{3n}F_6\left(\frac{M^2_{\chi^-_n}}{M^2_{S_m}}\right)\mathcal{D}^s_{2m}\mathcal{D}^{s*}_{4m}\frac{y_{e_1}}{g_2}. \quad (36)$$

It clearly has the $\mu^*_1B_2$ combination with an electron Yukawa suppression, and is thus smaller than expression (35). It is confirmed by our numerical calculation. The result we mentioned above is also discussed in Ref. [13]. The expression (33) becomes

$$\sum_{n=1}^{5}\sum_{m=1}^{5} -\boldsymbol{U}^*_{23}\boldsymbol{V}_{1n}M_{\chi^-_n}\boldsymbol{U}^*_{2n}F_6\left(\frac{M^2_{\chi^-_n}}{M^2_{S_m}}\right)\mathcal{D}^s_{2m}\mathcal{D}^{s*}_{4m}\frac{y_{e_2}}{g_2}, \quad (37)$$

and we have the $\mu^*_1B_2$ combination with a muon Yukawa suppression. The expression (34) becomes

$$\sum_{n=1}^{5}\sum_{m=1}^{5} -\boldsymbol{U}_{24}\boldsymbol{V}^*_{1n}M_{\chi^-_n}\boldsymbol{U}_{2n}F_6\left(\frac{M^2_{\chi^-_n}}{M^2_{S_m}}\right)\mathcal{D}^s_{3m}\mathcal{D}^{s*}_{2m}\frac{y_{e_1}}{g_2}, \quad (38)$$

and we have the $B^*_1\mu_2$ combination with an electron Yukawa suppression. We expect that this contribution is smaller than in expression (37), because it has a larger Yukawa suppression.

In summary, using an approximate formula of mass eigenstate couplings, one can only obtain the expression (35) and (36). However, in this paper, we take all contributions into account including diagrams with Higgsinos and winos on the external legs. Therefore, additional contributions, such as the expression (37) and (38) in

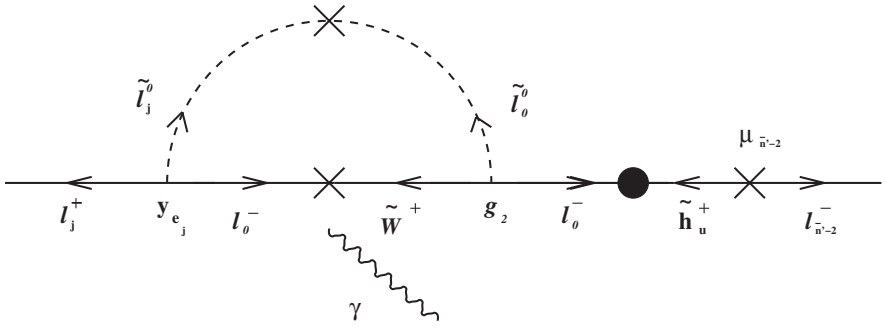

FIG. 8. The charginolike loop diagram contributes to the leptonic radiative decay due to $B_j\mu^*_{\bar{n}'-2}$ combination, where $\bar{n}' - 2 < j$.

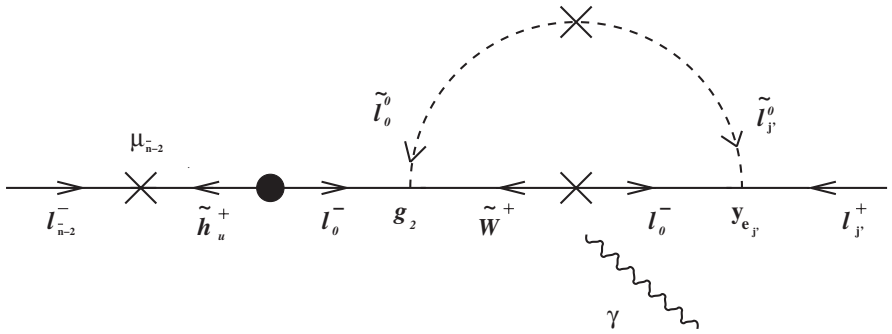

FIG. 9. The charginolike loop diagram contributes to the leptonic radiative decay due to $B^*_{j'}\mu_{\bar{n}-2}$ combination, where $j' < \bar{n} - 2$.

this case, would be obtained. If we consider the $B^*_1\mu_2$ combination, the dominant term still comes from expression (35), since the new contribution, expression (38), has an electron Yukawa suppression, while expression (35) only has a muon Yukawa suppression. However, the situation would be totally changed in the combination of $\mu^*_1 B_2$, since the expression (36) has an electron Yukawa suppression while the new contribution, expression (37), only has a muon Yukawa suppression. As a result, our exact formula made the allowed region of the (B_2, μ_1) parameter space more stringent than that in Ref. [13]. We give contours of $\mathrm{Br}(\mu \to e\gamma)$ in the real (B_2, μ_1) plane in Fig. 10. The solid lines represent the results obtained by using the exact mass eigenstate couplings, while the dashed lines stand for the results obtained by using the approximate ones. Likewise, the contour of $\mathrm{Br}(\tau \to e\gamma)$ is given in the real (B_3, μ_1) plane in Fig. 11. The present experimental limit is also shown and the allowed region at 90% C.L. is shaded.

The 90% C.L. upper limit on $|\mu^* B|$ or $|\mu B^*|$ type combinations (normalized by $|\mu_0|^3$, $|\mu_0| = 135$ GeV) is given by

$$\frac{|B^*_1\mu_2|}{|\mu_0|^3} < 6.5 \times 10^{-7}, \qquad \frac{|B_2\mu^*_1|}{|\mu_0|^3} < 7.1 \times 10^{-7},$$
$$\frac{|B^*_1\mu_3|}{|\mu_0|^3} < 1.4 \times 10^{-4}, \qquad \frac{|B_3\mu^*_1|}{|\mu_0|^3} < 1.5 \times 10^{-4}, \quad (39)$$
$$\frac{|B^*_2\mu_3|}{|\mu_0|^3} < 1.1 \times 10^{-4}, \qquad \frac{|B_3\mu^*_2|}{|\mu_0|^3} < 1.2 \times 10^{-4}.$$

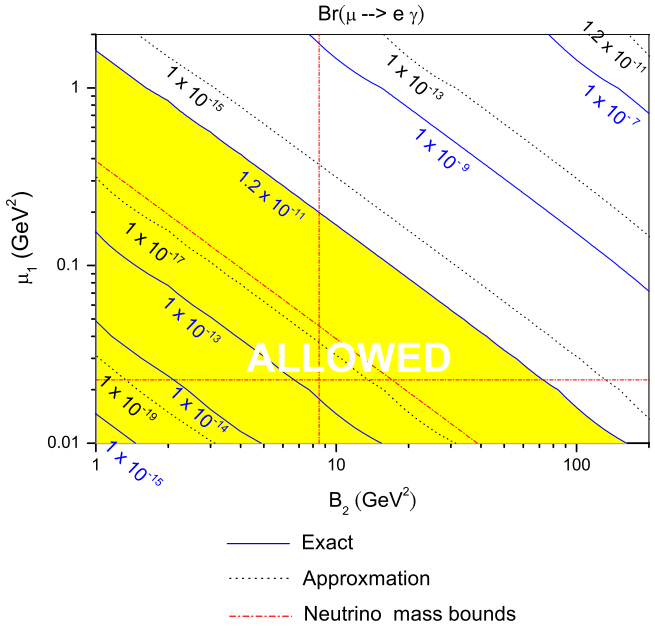

FIG. 10 (color online). Contours of $B(\mu \to e\gamma)$ in the (real) plane of (B_2, μ_1). The 90% C.L. allowed region is shaded. The solid lines represent the results obtained by using the exact mass eigenstate couplings, while the dashed lines stand for the results obtained by using the approximate ones. The dash-dotted (red) lines are neutrino mass bounds. Notice the MEG experiment targets probing the decay at 10^{-13}–10^{-14}.

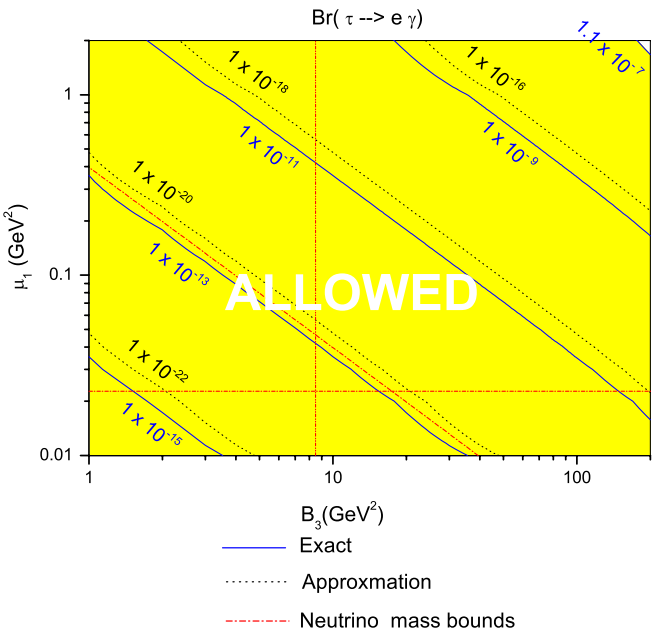

FIG. 11 (color online). Contours of $B(\tau \to e\gamma)$ in the (real) plane of (B_3, μ_1). The 90% C.L. allowed region is shaded. The solid lines represent the results obtained by using the exact mass eigenstate couplings, while the dashed lines stand for the results obtained by using the approximate ones. The dash-dotted (red) lines are neutrino mass bounds.

TABLE II. Summary of bounds on various combinations of two R-parity violating parameters, normalized by $|\mu_0| = 135$ GeV. The input parameters are as in Table I.

$\frac{\lvert\mu_3^*\lambda_{321}\rvert}{\lvert\mu_0\rvert}$, $\frac{\lvert\mu_1^*\lambda_{121}\rvert}{\lvert\mu_0\rvert}$, $\frac{\lvert\mu_3\lambda_{312}^*\rvert}{\lvert\mu_0\rvert}$, or $\frac{\lvert\mu_2\lambda_{212}^*\rvert}{\lvert\mu_0\rvert}$	$<2.1\times10^{-7}$
$\frac{\lvert\mu_2^*\lambda_{232}\rvert}{\lvert\mu_0\rvert}$, $\frac{\lvert\mu_1^*\lambda_{132}\rvert}{\lvert\mu_0\rvert}$, $\frac{\lvert\mu_3\lambda_{323}^*\rvert}{\lvert\mu_0\rvert}$, or $\frac{\lvert\mu_1\lambda_{123}^*\rvert}{\lvert\mu_0\rvert}$	$<7.0\times10^{-4}$
$\frac{\lvert\mu_2^*\lambda_{231}\rvert}{\lvert\mu_0\rvert}$, $\frac{\lvert\mu_1^*\lambda_{131}\rvert}{\lvert\mu_0\rvert}$, $\frac{\lvert\mu_3\lambda_{313}^*\rvert}{\lvert\mu_0\rvert}$, or $\frac{\lvert\mu_2\lambda_{213}^*\rvert}{\lvert\mu_0\rvert}$	$<8.5\times10^{-4}$
$\frac{\lvert B_1^*\mu_2\rvert}{\lvert\mu_0\rvert^3}$	$<6.5\times10^{-7}$
$\frac{\lvert B_2\mu_1^*\rvert}{\lvert\mu_0\rvert^3}$	$<7.1\times10^{-7}$
$\frac{\lvert B_1^*\mu_3\rvert}{\lvert\mu_0\rvert^3}$	$<1.4\times10^{-4}$
$\frac{\lvert B_3\mu_1^*\rvert}{\lvert\mu_0\rvert^3}$	$<1.5\times10^{-4}$
$\frac{\lvert B_2^*\mu_3\rvert}{\lvert\mu_0\rvert^3}$	$<1.1\times10^{-4}$
$\frac{\lvert B_3\mu_2^*\rvert}{\lvert\mu_0\rvert^3}$	$<1.2\times10^{-4}$
$\frac{\lvert\mu_1^*\mu_2\rvert}{\lvert\mu_0\rvert^2}$	$<3.7\times10^{-5}$
$\frac{\lvert\mu_1^*\mu_3\rvert}{\lvert\mu_0\rvert^2}$	$<4.7\times10^{-3}$
$\frac{\lvert\mu_2^*\mu_3\rvert}{\lvert\mu_0\rvert^2}$	$<3.6\times10^{-3}$
$\frac{\lvert B_3^*\lambda_{321}\rvert}{\lvert\mu_0\rvert^2}$, $\frac{\lvert B_1^*\lambda_{121}\rvert}{\lvert\mu_0\rvert^2}$, $\frac{\lvert B_3\lambda_{312}^*\rvert}{\lvert\mu_0\rvert^2}$, or $\frac{\lvert B_2\lambda_{212}^*\rvert}{\lvert\mu_0\rvert^2}$	$<1.3\times10^{-4}$
$\frac{\lvert B_2^*\lambda_{232}\rvert}{\lvert\mu_0\rvert^2}$, $\frac{\lvert B_1^*\lambda_{132}\rvert}{\lvert\mu_0\rvert^2}$, $\frac{\lvert B_3\lambda_{323}^*\rvert}{\lvert\mu_0\rvert^2}$, or $\frac{\lvert B_1\lambda_{123}^*\rvert}{\lvert\mu_0\rvert^2}$	$<1.4\times10^{-3}$
$\frac{\lvert B_2^*\lambda_{231}\rvert}{\lvert\mu_0\rvert^2}$, $\frac{\lvert B_1^*\lambda_{131}\rvert}{\lvert\mu_0\rvert^2}$, $\frac{\lvert B_3\lambda_{313}^*\rvert}{\lvert\mu_0\rvert^2}$, or $\frac{\lvert B_2\lambda_{213}^*\rvert}{\lvert\mu_0\rvert^2}$	$<1.9\times10^{-3}$

For a direct contrast, we also give the *incorrect* upper bounds obtained by using the approximate formula:

$$\frac{|B_2\mu_1^*|}{|\mu_0|^3} < 1.4\times10^{-4}, \qquad \frac{|B_3\mu_1^*|}{|\mu_0|^3} < 3.5\times10^{0},$$
$$\frac{|B_3\mu_2^*|}{|\mu_0|^3} < 2.3\times10^{-3}.$$

We can see clearly that the ratio between the limit of $\frac{|B_2\mu_1^*|}{|\mu_0|^3}$ and the correct one in Eq. (39) is approximately the ratio of $\frac{y_{e_2}}{y_{e_1}}$. Therefore, the difference of the experimental bounds between the exact formula (solid line) and the approximate formula (dashed line) in Fig. 10 is the result of different Yukawa suppressions, which is consistent with our analysis. If we take the expected improvement from the MEG experiment into account and assume $\mathrm{Br}(\mu \to e\gamma) < 10^{-14}$, we get

$$\frac{|B_1^*\mu_2|}{|\mu_0|^3} < 1.2\times10^{-8}, \qquad \frac{|B_2\mu_1^*|}{|\mu_0|^3} < 1.3\times10^{-8}.$$

TABLE III. Effects of parameter variations of interest, on the bounds of $|\mu_1^*\lambda_{121}|\cdot(135\ \mathrm{GeV})^{-1}$ and $|\mu_1^*B_2|\cdot(135\ \mathrm{GeV})^{-3}$. Note that the fixed mass scale of 135 GeV is used for normalization to extract numerical bounds.

Parameter changes	Normalized numerical bounds $\frac{\lvert\mu_1^*\lambda_{121}\rvert}{(135\ \mathrm{GeV})}$	$\frac{\lvert\mu_1^*B_2\rvert}{(135\ \mathrm{GeV})^3}$
Original inputs of Table I	$<2.1\times10^{-7}$	$<7.1\times10^{-7}$
(i) $\tilde{m}_L^2 = \mathrm{diag}\{20\,000, 500^2, 500^2, 500^2\}\ \mathrm{GeV}^2$, $\tilde{m}_E^2 = \mathrm{diag}\{500^2, 500^2, 500^2\}\ \mathrm{GeV}^2$		
$\mu_0 = 500$ GeV	$<7.5\times10^{-6}$	$<2.1\times10^{-4}$
$\mu_0 = 250$ GeV	$<2.7\times10^{-6}$	$<3.0\times10^{-5}$
$\mu_0 = 135$ GeV	$<1.3\times10^{-6}$	$<7.1\times10^{-6}$
$\mu_0 = -135$ GeV	$<1.3\times10^{-6}$	$<7.3\times10^{-6}$
$\mu_0 = -250$ GeV	$<2.9\times10^{-6}$	$<3.1\times10^{-5}$
$\mu_0 = -500$ GeV	$<8.2\times10^{-6}$	$<2.1\times10^{-4}$
(ii) $M_1 = \frac{1}{2}M_2 = 500$ GeV	$<1.2\times10^{-6}$	$<4.5\times10^{-6}$
(iii) $\tilde{m}_L^2 = 20\,000\times\mathrm{diag}\{1,1,1\}\ \mathrm{GeV}^2$	$<2.9\times10^{-7}$	$<9.7\times10^{-7}$
$\tilde{m}_L^2 = \mathrm{diag}\{20\,000, 1000^2, 1000^2, 1000^2\}\ \mathrm{GeV}^2$	$<3.0\times10^{-6}$	$<2.1\times10^{-5}$
(iv) $\tilde{m}_E^2 = 20\,000\times\mathrm{diag}\{1,1,1\}\ \mathrm{GeV}^2$	$<2.1\times10^{-7}$	$<7.3\times10^{-7}$
$\tilde{m}_E^2 = \mathrm{diag}\{1000^2, 1000^2, 1000^2\}\ \mathrm{GeV}^2$	$<2.2\times10^{-7}$	$<8.7\times10^{-7}$
(v) $\tilde{m}_L^2 = \mathrm{diag}\{20\,000, 500^2, 500^2, 500^2\}\ \mathrm{GeV}^2$, $\tilde{m}_E^2 = \mathrm{diag}\{500^2, 500^2, 500^2\}\ \mathrm{GeV}^2$		
$\mu_0 = 135$ GeV, $\tan\beta = 2$	$<8.7\times10^{-7}$	$<2.6\times10^{-3}$
$\tan\beta = 10$	$<1.1\times10^{-6}$	$<1.1\times10^{-4}$
$\tan\beta = 50$	$<1.3\times10^{-6}$	$<4.5\times10^{-6}$
$\mu_0 = 250$ GeV, $\tan\beta = 2$	$<1.7\times10^{-6}$	$<1.2\times10^{-2}$
$\tan\beta = 10$	$<2.4\times10^{-6}$	$<4.7\times10^{-4}$
$\tan\beta = 50$	$<2.7\times10^{-6}$	$<1.9\times10^{-5}$
$\mu_0 = 500$ GeV, $\tan\beta = 2$	$<3.9\times10^{-6}$	$<8.3\times10^{-2}$
$\tan\beta = 10$	$<6.4\times10^{-6}$	$<3.2\times10^{-3}$
$\tan\beta = 50$	$<7.5\times10^{-6}$	$<1.3\times10^{-4}$

Notice that this constraint is even more stringent than the one from neutrino masses as you can see in Fig. 10.

C. Parameter variations

In this section, we illustrate the effects of varying the input SUSY parameters on the bounds, using $|\mu_1^* \lambda_{121}|$ and $|\mu_1^* B_2|$ as examples. The results are summarized in Table III. In the table, we list the variation of the μ_0 and the M_1 in parts i and ii, respectively. Our numerical results show that the bound is most stringent for small $|\mu_0|$ in both $|\mu_1^* \lambda_{121}|$ and $|\mu_1^* B_2|$ cases. In addition, the increase of M_1 also weakens the bound. These results are reasonable since increasing μ_0 and $M_1 = \frac{1}{2} M_2$ essentially increases the chargino and neutralino masses. In the case of $|\mu_1^* \lambda_{121}|$, the dominant diagram involves mainly the $\tilde{l}_2^0$, while the $|\mu_1^* B_2|$ case involves the mixing between $\tilde{l}_2^0$ and $\tilde{l}_0^0$. Therefore, varying $\tilde{m}_E^2$ does not have much effect on the bounds while varying the corresponding entries in $\tilde{m}_L^2$ changes the bounds significantly (see parts iii and iv).

Finally, part v of Table III shows the $\tan\beta$ dependence of the results. From the table we can see that varying $\tan\beta$ has only a little effect on $|\mu_1^* \lambda_{121}|$, but a rather significant effect on $|\mu_1^* B_2|$. Although the subdominant contributions mentioned in Sec. IV B involve the Yukawa couplings, and thus have the $\frac{1}{\cos\beta}$ dependence, the dominant contributions do not have the $\tan\beta$ dependence [13]. As a result, the lack of sensitivity to $\tan\beta$ in the former case is to be expected. In the latter case, the numerical result shows that the bound has a strong dependence on $\tan\beta$. There are two sources that result in this dependence. The first one is the $\frac{1}{\cos\beta}$ dependence of the Yukawa coupling. The other is the explicit $\tan\beta$ dependence of the dominant terms mentioned in Sec. IV C. Figure 12 shows a contour plot of the experimental bound of $B(\mu \to e\gamma)$ in the (real) plane of (B_2, μ_1) for various values of $\tan\beta$. It not only shows the $\tan\beta$ dependence of the results, but also illustrates that the experimental bound gives a more stringent constraint in the large $\tan\beta$ region.

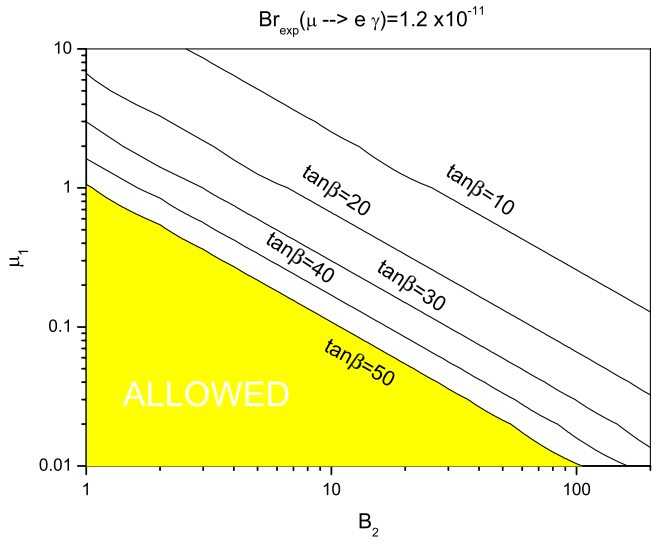

FIG. 12 (color online). Contours of the experimental bound of $B(\mu \to e\gamma)$ in the (real) plane of (B_2, μ_1) with different values of $\tan\beta$, ranging from 10 to 50, among which $\tan\beta = 50$ gives the most stringent constraint and the corresponding 90% C.L. allowed region is shaded.

V. CONCLUSION

In this paper, we have given explicit formulas and detailed discussions on the full one-loop contribution to the radiative decay of μ and τ, namely, $\mu \to e\gamma$, $\tau \to e\gamma$, and $\tau \to \mu\gamma$ for the generic supersymmetric SM (without R parity). We use the exact formula of the mass eigenstate couplings to calculate the branching ratios of these leptonic radiative decay processes and compare them with the results obtained in an earlier approximation in Ref. [13]. In some combinations of RPV parameters, the results obtained by using these two approaches are exactly the same such as $\mu_1 \lambda_{123}^*$, $\mu_1^* \lambda_{132}$, $\mu_2 \lambda_{213}^*$, $\mu_2^* \lambda_{231}$, $\mu_3^* \lambda_{321}$, $\mu_3 \lambda_{312}^*$, and all $B^* \lambda$ and $B \lambda^*$ type combinations. The dominant terms of the other $\mu^* \lambda$ or $\mu \lambda^*$ combinations such as $\mu_2 \lambda_{212}^*$, $\mu_1^* \lambda_{121}$, $\mu_3 \lambda_{313}^*$, $\mu_1^* \lambda_{131}$, $\mu_3^* \lambda_{323}$, and $\mu_2 \lambda_{232}^*$ are still the same in the two methods, but the subdominant terms come from a new contribution. In the $B^* \mu$ or $B \mu^*$ contributions, the dominant contributions of $B_1^* \mu_2$, $B_1^* \mu_3$, and $B_2^* \mu_3$ are the same in the exact and approximate formulas. However, the dominant contributions of $\mu_1^* B_2$, $\mu_1^* B_3$, and $\mu_2^* B_3$ are totally new. The upper bound on these combinations obtained from the experimental limit are

$$\frac{|B_2 \mu_1^*|}{|\mu_0|^3} < 7.1 \times 10^{-7}, \qquad \frac{|B_3 \mu_1^*|}{|\mu_0|^3} < 1.5 \times 10^{-4},$$

$$\frac{|B_3 \mu_2^*|}{|\mu_0|^3} < 1.2 \times 10^{-4}.$$

As a result, our exact formulas impose more stringent constraints on the admissible region of parameter spaces for the GSSM, or SUSY without R parity. If we also consider the expected improvement from the MEG experiment and assume $\mathrm{Br}(\mu \to e\gamma) < 10^{-14}$, we could get even more stringent constraints on the $B_2^* \mu_1$ combination

$$\frac{|B_2 \mu_1^*|}{|\mu_0|^3} < 1.3 \times 10^{-8}.$$

The constraint is even more stringent than the naive constraint from neutrino masses imposed here, which indicates a very encouraging scenario for future probing of the leptonic radiative decay and may be as well as the τ decays. A more involved analysis will have to be performed on the full model parameter space matching the radiative decays to neutrino mass generations. We want to highlight though that the scale for the actual neutrino masses is not expected to be reduced while probes on the

leptonic radiative decays, and for that matter the other lepton number/flavor violating decays, can be improved. That makes the latter a promising ground to further explore models like SUSY without R parity with rich lepton number/flavor violating structures.

ACKNOWLEDGMENTS

The work of O. K. is partially supported by research Grant No. 96-2112-M-008-007-MY3 of the NSC of Taiwan. The authors would like to thank Katherine Sutton for editing this paper.

[1] B. Aubert *et al.* (*BABAR* Collaboration), Phys. Rev. Lett. **95**, 041802 (2005).
[2] B. Aubert *et al.* (*BABAR* Collaboration), Phys. Rev. Lett. **96**, 041801 (2006).
[3] M. L. Brooks *et al.* (MEGA Collaboration), Phys. Rev. Lett. **83**, 1521 (1999).
[4] A. Maki, AIP Conf. Proc. **981**, 363 (2008).
[5] S. R. Choudhury, A. S. Cornell, A. Deandrea, N. Gaur, and A. Goyal, Phys. Rev. D **75**, 055011 (2007).
[6] M. Blanke, A. J. Buras, B. Duling, A. Poschenrieder, and C. Tarantino, J. High Energy Phys. 05 (2007) 013.
[7] L. Calibbi, A. Faccia, A. Masiero, and S. K. Vempati, Phys. Rev. D **74**, 116002 (2006).
[8] L. Calibbi, A. Faccia, A. Masiero, and S. K. Vempati, J. High Energy Phys. 07 (2007) 012.
[9] O. C. W. Kong, Int. J. Mod. Phys. A **19**, 1863 (2004).
[10] M. Bisset, O. C. W. Kong, C. Macesanu, and L. H. Orr, Phys. Lett. B **430**, 274 (1998).
[11] M. Bisset, O. C. W. Kong, C. Macesanu, and L. H. Orr, Phys. Rev. D **62**, 035001 (2000).
[12] O. C. W. Kong, J. High Energy Phys. 09 (2000) 037.
[13] K. Cheung and O. C. W. Kong, Phys. Rev. D **64**, 095007 (2001).
[14] K. Choi, E. J. Chun, and K. Hwang, Phys. Lett. B **488**, 145 (2000).
[15] Y.-Y. Keum and O. C. W. Kong, Phys. Rev. Lett. **86**, 393 (2001); Phys. Rev. D **63**, 113012 (2001); K. Choi, E. J. Chun, and K. Hwang, Phys. Rev. D **63**, 013002 (2000). See also C.-C. Chiou, O. C. W. Kong, and R. Vaidya, Phys. Rev. D **76** 013003 (2007).
[16] O. C. W. Kong and R. Vaidya, Phys. Rev. D **72**, 014008 (2005). See also **71**, 055003 (2005).
[17] I. H. Lee, Phys. Lett. **138B**, 121 (1984); Nucl. Phys. **B246**, 120 (1984).
[18] B. de Carlos and P. L. White, arXiv:hep-ph/9609304.
[19] S. Eidelman *et al.* (Particle Data Group), Phys. Lett. B **592**, 1 (2004).
[20] O. C. W. Kong, Mod. Phys. Lett. A **14**, 903 (1999).
[21] S. K. Kang and O. C. W. Kong, Phys. Rev. D **69**, 013004 (2004).